Chapter 2

Osteocyte Apoptosis-Induced Bone Resorption in Mechanical Remodeling Simulation – Computational Model for Trabecular Bone Structure

Ji Yean Kwon, Hisashi Naito, Takeshi Matsumoto and Masao Tanaka

Additional information is available at the end of the chapter

http://dx.doi.org/10.5772/50301

1. Introduction

Biomechanical function is one of primal concern in musculo-skeletal system supporting our body as a whole. The functional adaptation of bone to the mechanical environment has been most interesting topic in bone mechanics. We have proposed the generalized model of bone remodeling simulation considering osteocyte apoptosis and targeted remodeling. These are important factors of bone metabolism under physiological and pathological conditions. This remodeling model has the capability to speculate the changes in the trabecular bone structures under various loading conditions. In this chapter, we describe how the osteocyte apoptosis-induced bone resorption has importance in computer simulations for disuse-meditated trabecular bone remodeling resulting in the osteoporotic bone structure in the human femur.

1.1. Cells activity in bone

Bone tissue is the component of the skeletal system supporting human body. Bone structure is continuously renewed by remodeling, that is, the alternately-repeated events of local bone resorption and formation. Three mature cell types of osteoblasts, osteoclasts and osteocytes play crucial roles in bone remodeling process. Bone metabolism is regulated by bone cells which respond to various environmental signals coming from chemical, magnetic, electrical and mechanical stimuli (Klein-Nulend et al., 2005).

Osteoblast are bone forming cells that synthesize and secrete bone matrix, participate in the calcification and formation of bone, and regulate the flux of calcium and phosphate in and

out of bone. Osteoclasts are multinucleated giant cells; their role is to resorb bone. Actively resorbing osteoclasts are usually found in cavities on bone surfaces, called resorption cavities. Osteocytes are the most abundant cell type in mature bone. During bone formation some osteoblasts are left behind in the newly formed osteoid as osteocytes when the bone formation moves on. The embedded osteoblast in lacunae differentiate into osteocytes by losing much of their organelles but acquiring long, slender processes encased in the lacunar-canulicular network that allow contact with earlier incorporated osteocytes and with osteoblast and bone lining and periosteal cells lining the bone surface and the vasculature. The osteocytes are the cells best placed to sense the magnitude and distribution of strains. They are strategically placed both to respond to changes in mechanical strain and to disseminate fluid flow to transduce information to surface cells of the osteoblastic lineage via their network of canalicular processes and communicating gap junctions (Cowin, 2001).

1.2. Mechanical stimuli in bone

Mechanical stimuli are one of the important regulation factors of bone remodeling. According to recent findings, osteocytes might play a role in the mechanical regulation of bone, receiving mechanical input signals and transmitting these stimuli to other cells in bone. Osteocyte is believed to comprise a sensory network that monitors mechanical load and tissue damage, and triggers appropriate adaptive responses, either formation or resorption. Mechanisms by which osteocytes could sense mechanical load have been understood by means of fluid movements throughout the lacunar-canalicular system, with some combination of shear stress and streaming potentials providing the proximate stimuli. The relations between mechanical stimuli and mature bone have been examined by experimental studies. There are suggested that higher rates of mechanical loading would evoke grater adaptive responses than lower rates of loading in mature bone (LaMonte et al., 2005). Exercise can substantially alter the physical states of a bone and generate adaptive responses. In a randomized controlled clinical trial, Fuchs et al.(2001) showed that, in jumpers, jumping significantly increases bone mineral content in femoral neck and lumbar skeleton relative to controls. McKay et al. (2000) found that jumping three times weekly for 8 months significantly augmented a real bone mineral density in the femoral trochanteric region. These studies have hypothesized that loading induced stimuli is the main signal-generating factor and play a key role in mechanobiology. However, disuse uncouples bone formation from resorption, leading to increased porosity, decreased bone geometrical properties, and decreased bone mineral content which compromises bone mechanical properties and increases fracture risk. The removal of routine bone stresses (e.g. from immobilization, inactivity, or reduced gravity) has deleterious consequences on bone integrity. Reduced skeletal loading causes net bone loss by unbalancing bone formation and bone resorption (Takata and Yasui, 2001; Caillot-Augusseau et al., 1998). Rat hindlimb immobilization, human spaceflight, and human bedrest can all cause increased bone resorption and decreased bone formation (Caillot-Augusseau et al., 1998; Weinreb et al., 1989; Li et al., 2005; McGee et al., 2008). Therefore, the process of mechanotransduction of bone, the conversion of a mechanical stimulus into a biochemical response, is known to occur in osteoblast, osteoclast and osteocytes in response to it.

1.3. Mechanical stimuli and osteocyte apoptosis

It is well recognized that the origin of osteocyte is osteoblasts embedded in its own matrix and some osteocytes die eventually (apoptosis). Aging, loss of estrogen, loading, and chronic glucocorticoid administration is known to increase osteocyte apoptosis and loading decreases the proportion of apoptotic osteocyte in cortical bone in rats (Noble et al., 2003; Gu et al., 2005; Delgado-Calle et al., 2011; Kennedy et al., 2012). These studies investigated the role of osteocytes in the control of loading related remodeling and they exhibited the effects on osteocyte viability of mechanical loading applied to the bone. Osteocyte apoptosis triggers osteoclast precursor recruitment to initiate bone resorption, whether it is induced by weightlessness or fatigue loading and precedes osteoclast resorption. An osteoclast/osteoblast-dependent process related on the osteocytes population may participate in making the decision as to where and when a new remodeling cycle will be initiated. That is, osteocyte network could be considered the main sensor of loads. To take these observations into account, Frost proposed the concept of mechanostat (Duncan & Turner, 1995; Frost, 2003; Hughes et al., 2010). According to this concept, the authors have proposed the mathematical model for bone remodeling described in the following section.

2. Bone remodeling simulation

To develop the computer simulation model of bone remodeling considering bone metabolism macroscopically, this section describes the bone remodeling model referring to the strain-based mechanostat theory submitted by Harold Frost and refined more than 5 decades. Physiological, low, and high strain ranges were defined in mechanostat theory, and different mechanisms were considered to describe the mechanical surface remodeling of trabecular architecture resulting in the structural change (Kwon et al., 2010a).

The following was assumed as the result of a remodeling turnover for each strain range: 1) in the physiological strain range, the occurrence of bone resorption or formation depends on the degree of the local stress non-uniformity; 2) in the low strain range, only bone resorption occurs owing to osteocyte apoptosis and its frequency increases with decreasing strain; 3) in the high strain range, only bone formation occurs by targeted remodeling and its frequency increases with strain. Each window is distinguished by threshold values of equivalent strain ε_e in the context of the mechanostat theory, and low, physiological, and high strain range correspond to the strain ranges of ε_e smaller than ε_{du}, between ε_{pl} - ε_{pu} and larger than ε_{ol} (Fig 1).

Trabecular architecture is discretized using voxel finite elements, as schematically shown in Fig. 2. The trabecular surface movement by remodeling is expressed by adding and removing voxel elements on the surface according to the mechanical stress/strain conditions determined by a finite element analysis. Each trabecular element was classified by equivalent strain into low, physiological, and high strain range. Bone surface remodeling was assumed to occur according to the mathematical models of each window described in the following sections in detail.

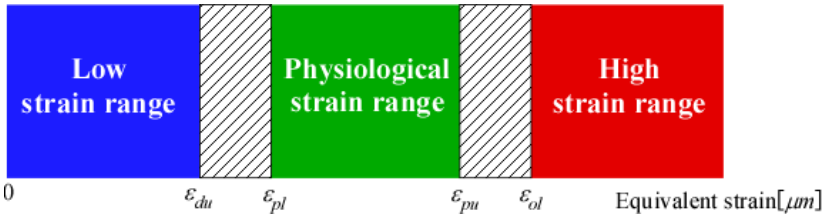

Figure 1. Strain ranges categorized by the equivalent strain and in-between transition ranges.

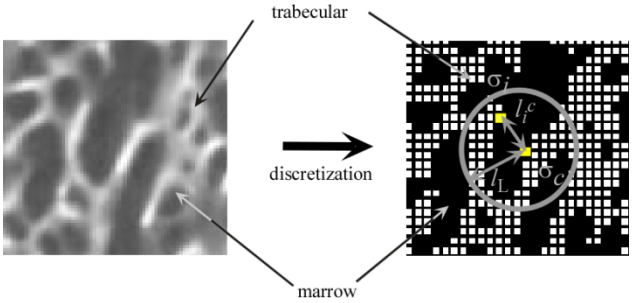

Figure 2. Discretized trabecular bone.

2.1. Physiological strain range: Mechanical adaptation by remodeling

In the physiological strain range ($\varepsilon_{pl} < \varepsilon_c < \varepsilon_{pu}$), the non-uniformity of the stress/strain distribution was taken as driving stimuli (Adachi et al., 1997). For the voxel representing a point c on bone surface, the magnitude of local stress non-uniformity Γ_c was quantified as

$$\Gamma_c = \ln\left(\sigma_c \sum_i^N w\left(l_i^c\right) \Big/ \sum_i^N w\left(l_i^c\right)\sigma_i\right) \tag{1}$$

where σ_c denotes the stress at the point c and σ_i denotes the representative stress at a point i with the distance l_i^c from c. The function $w(l_i^c)$ is described as

$$w\left(l_i^c\right) = \begin{cases} 1 - l_i^c / l_L & \left(0 \le l_i^c < l_L\right) \\ 0 & \left(l_L \le l_i^c\right) \end{cases} \tag{2}$$

defining a positive weight for the neighboring point i within the limit of sensing distance l_L from the point c under consideration. This represents the sensory integration by osteocyte network.

The probability $f(\Gamma_c)$ of bone resorption or formation at the point c is described by

$$f\left(\Gamma_c\right) = \begin{cases} P_f\left(\Gamma_c\right) & \left(0 < \Gamma_c\right) \\ 0 & \left(\Gamma_c = 0\right) \\ -P_r\left(\Gamma_c\right) & \left(\Gamma_c < 0\right) \end{cases} \tag{3}$$

$$P_f(\Gamma_c)=\begin{cases}\dfrac{1}{2}\left\{\sin\pi\left(\dfrac{\Gamma_c}{\Gamma_u}-\dfrac{1}{2}\right)+1\right\} & (0<\Gamma_c\le\Gamma_u)\\ 1 & (\Gamma_u<\Gamma_c)\end{cases} \tag{4}$$

$$P_r(\Gamma_c)=\begin{cases}\dfrac{1}{2}\left\{\sin\pi\left(\dfrac{\Gamma_c}{\Gamma_l}-\dfrac{1}{2}\right)+1\right\} & (\Gamma_l\le\Gamma_c<0)\\ 1 & (\Gamma_c<\Gamma_l)\end{cases} \tag{5}$$

where Γ_u and Γ_l denote the lower and upper threshold values, respectively. More specifically, voxel elements are added around the surface point c when $f(\Gamma_c) = 1$, and the voxel c is subtracted when $f(\Gamma_c)=-1$. The case of $f(\Gamma_c)=0$ represents local remodeling equilibrium and no change occurs at and around c. Moreover, in the cases of $0 < \Gamma_c \le \Gamma_u$ and $\Gamma_l \le \Gamma_c < 0$, bone formation and resorption occurs stochastically according to probability $f(\Gamma_c)$. In this physiological strain range, the activation frequency AF_f or AF_r, defined as a relative rate for bone formation or resorption, is set to unity, i.e., $AF_f = AF_r = 1$.

2.2. Low strain range: Osteocyte apoptosis- induced bone resorption

In the low strain range ($\varepsilon_c < \varepsilon_{du}$), only osteocyte apoptosis-accelerated bone resorption is assumed to occur (Noble et al. 2003; Gu et al., 2005; Li et al. 2005). The probability of bone resorption is unity, i.e.,

$$P_{LS} = 1 \quad \text{and} \quad f(\Gamma_c) = -1. \tag{6}$$

The degree of osteocyte apoptosis increases with the decrease of strain. Thus, the activation frequency for bone resorption AF_r is also elevated with the decrease of strain and is described by

$$AF_r(\varepsilon_c)=\begin{cases}AF_{r\max} & (0<\varepsilon_c<\varepsilon_{\min})\\ \left(\dfrac{\varepsilon_{du}}{\varepsilon_c}\right)^a & (\varepsilon_{\min}<\varepsilon_c<\varepsilon_{du}),\ a=\dfrac{\ln AF_{r\max}}{\ln(\varepsilon_{du}/\varepsilon_{\min})}\end{cases} \tag{7}$$

where AF_r reaches the maximum AF_{rmax} at $\varepsilon_c = \varepsilon_{min}$.

2.3. High strain range: Targeted remodeling by over use

In the high strain range ($\varepsilon_{ol} < \varepsilon_c$), only bone formation is assumed to occur. The probability of bone formation as the result of remodeling turnover is unity, i.e.,

$$P_{HS} = 1 \quad \text{and} \quad f(\Gamma_c) = 1. \tag{8}$$

Bone formation in high strain range undergoes the targeted remodeling mechanism (Burr, 2002; Da Costa Gómez et al., 2005), and thus the activation frequency for bone formation AF_f is also elevated with the increase of strain and is described by

$$AF_f(\varepsilon_c)=\begin{cases}\dfrac{AF_{fmax}-1}{2}\left\{sin\pi\left(\dfrac{\varepsilon_c-\varepsilon_{ol}}{\varepsilon_{max}-\varepsilon_{ol}}-\dfrac{1}{2}\right)+1\right\} & \left(\varepsilon_{ol}\le\varepsilon_c<\varepsilon_{max}\right)\\ AF_{fmax} & \left(\varepsilon_c\ge\varepsilon_{max}\right)\end{cases} \tag{9}$$

where AF_f reaches the maximum AF_{fmax} at $\varepsilon_c=\varepsilon_{max}$. It is noted that the pathological overuse is not considered here and the upper limit ε_{max} is enforced for ε_c in high strain range.

2.4. Integrated mathematical model and simulation procedures for bone remodeling

The mathematical models of bone remodeling established in low, physiological, and high strain ranges were integrated by introducing transition regions. In the transition regions between low and physiological range ($\varepsilon_{du}<\varepsilon_c<\varepsilon_{pl}$) or between physiological and high range ($\varepsilon_{pu}<\varepsilon_c<\varepsilon_{ol}$), the probabilities of bone resorption or formation in each window were combined as a linearly weighed sum as given by Eqs. (10)-(12) resulting the resultant probability f^* of bone resorption/formation.

$$\mathrm{f}^*(\Gamma_c,\varepsilon_c)=\begin{cases}-\mathrm{P_{LS}} & \left(\varepsilon_c<\varepsilon_{du}\right)\\ -\left(1-\dfrac{\varepsilon_c-\varepsilon_{du}}{\varepsilon_{pl}-\varepsilon_{du}}\right)\mathrm{P_{LS}}+\dfrac{\varepsilon_c-\varepsilon_{du}}{\varepsilon_{pl}-\varepsilon_{du}}f(\Gamma_c) & \left(\varepsilon_{du}<\varepsilon_c<\varepsilon_{pl}\right)\\ f(\Gamma_c) & \left(\varepsilon_{pl}<\varepsilon_c<\varepsilon_{pu}\right)\\ \left(1-\dfrac{\varepsilon_c-\varepsilon_{pu}}{\varepsilon_{ol}-\varepsilon_{du}}\right)f(\Gamma_c)+\dfrac{\varepsilon_c-\varepsilon_{pu}}{\varepsilon_{ol}-\varepsilon_{pu}}\mathrm{P_{HS}} & \left(\varepsilon_{pu}<\varepsilon_c<\varepsilon_{ol}\right)\\ \mathrm{P_{HS}} & \left(\varepsilon_{ol}<\varepsilon_c\right)\end{cases} \tag{10}$$

$$P_f^*=f^*(\Gamma_c,\varepsilon_c)\,(f^*(\Gamma_c,\varepsilon_c)\ge 0) \tag{11}$$

$$P_r^*=f^*(\Gamma_c,\varepsilon_c)\,(f^*(\Gamma_c,\varepsilon_c)<0) \tag{12}$$

Using this integrated model, trabecular bone structure was simulated by the following procedures.

1. The initial shape of the trabecular bone is discretized by voxel finite elements and Young's modulus and Poisson's ratio are given.
2. The equivalent stress and strain distributions are determined under a given mechanical boundary condition.
3. The probabilities P_f* and P_r* of bone formation or resorption are calculated for every voxel on bone surface by Eqs. (10) - (12).
4. The activation frequency AF_f and AF_r of bone formation or resorption are calculated for every voxel on bone surface by Eqs. (7) and (9). These are rounded to the nearest integer number and truncated by AF_{fmax} or AF_{rmax}.
5. Bone surface movement (voxel removal or addition) is determined stochastically based on P_f* and P_r*.

6. For voxels with activation frequency AF_r or AF_f larger than one, the same surface movements in procedure (4) are repeated AF_r or AF_f times.
7. Procedures (2)-(6) are repeated until equilibrium is achieved.

3. Simulation of trabecular bone structures for human proximal femur

3.1. Voxel FE model of human proximal femur

The three-dimensional profile of human proximal femur is reconstructed using computed tomography (female, 70 years, hip osteoarthritis), the resolution of the images was 0.7 mm so that the entire volume could be captured with slice image of 512×512 cubic voxels. As the random initial trabecular structure in proximal femur, an artificial trabecular structure was given by the random-placement of hollow spheres with inside and outside diameters of 2100 and 4200 μm, respectively (Kwon et al., 2010a). One voxel was transferred to one finite element of eight node brick element. The isotropic elastic body with Young's modulus of 20.0 GPa and Poisson's ratio of 0.3 was assumed for trabecular bone material. The cortical outer surface was fixed throughout the remodeling simulation, and the intra-structure, from the head to mid-shaft, was remodeled in accordance with the same remodeling procedure. The fixed boundary conditions are imposed on the distal end. In the daily loading condition, we considered the one-legged stance, abduction, and adduction, which accounted for 50, 25, and 25% of this condition as illustrated in Fig. 3. The loading magnitudes and frequencies of these three stances were shown in Table 1 (Beaupré et al., 1990; Adachi et al., 1997). The extreme ranges of motion of abduction and adduction were assumed. The trabecular structure obtained under this daily loading condition was referred to as the normal structure and also used for the initial structure for the remodeling simulation under reduced weight-bearing conditions (Kwon et al., 2010b).

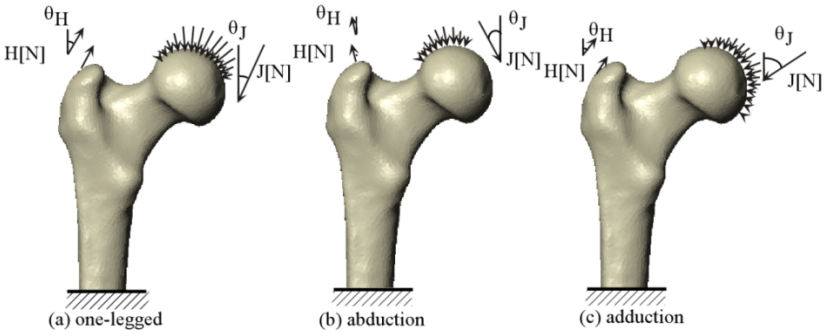

Figure 3. Standard weight-bearing cases at each stance (daily-loading condition).

3.2. Healthy trabecular structures in proximal femur

The simulation results from initial random structure to an equilibrium state are shown in Fig. 4. In the diaphyseal region, random inner structures disappeared whereas the thickness of cortical bone increased with simulation step to the similar level observed in CT image (Fig.

4(g)). On the other hand, trabecular bone in the metaphyseal region, showing an isotropical random pattern at the initial (Fig. 4(a)), changed to an anisotropic, non-uniform structure. Bone volume was maintained in femoral head region A but decreased in neck region B reproducing Ward's triangle characteristic of trabecular structure in the proximal femur.

	One-legged (*n=ol*)	Abduction (*n=ab*)	Adduction (*n=ad*)
Frequency f_n [cycle/day]	6000	2000	2000
θ_J	24°	-15°	56°
J [N]	2317	1158	1548
θ_H	28°	-8°	35°
H [N]	703	351	468

Table 1. Standard magnitude of force and frequency at each stance (daily-loading condition).

Regions A and B were subdivided to blocks of 10×10×10 voxels to compare local bone volume fraction in each block with local bone mineral density(Duchemin et al., 2008) i.e., averaged bone mineral density in the corresponding CT voxels referring to the phantoms of trabecular bone (B-mas 200). Trabecular bone volume fraction was correlated significantly with bone mineral density as shown in Fig. 5.

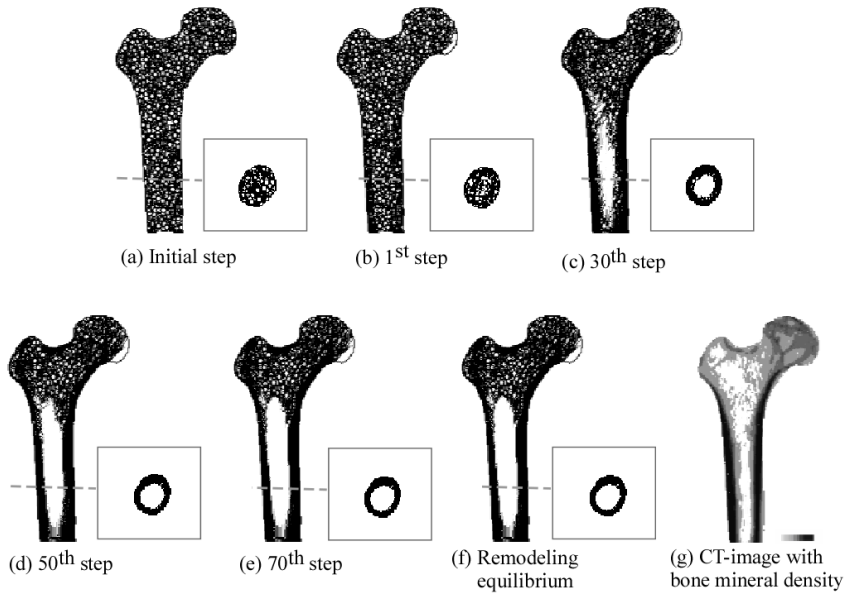

Figure 4. Simulated trabecular structure in human proximal femur and CT-image (Subject #1).

3.3. Disuse mediated change in proximal femur

To estimate the effect of weightlessness-induced osteocyte apoptosis in trabecular bone in proximal femur, two reduced weight-bearing conditions were considered here: the infrequent

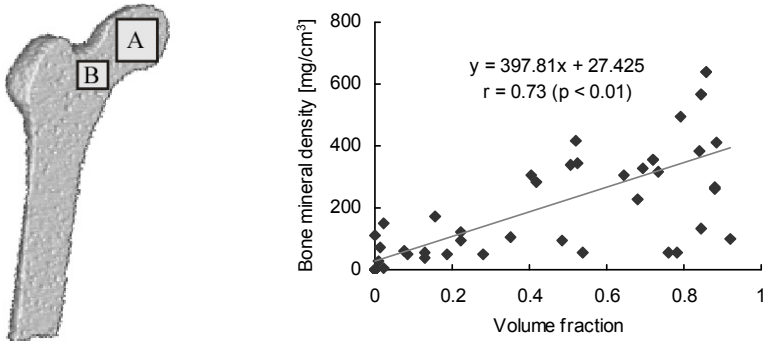

Figure 5. Bone mineral density vs. simulated volume fraction.

walking and the cane-assisted walking. In the infrequent walking condition, we wedged the interval with no loading into the daily loading condition; that is, the infrequent walking condition consisted of unloading of zero load and a part of the daily loading conditions. The proportion of unloading interval changed from 10 to 70% while the ratio of one-legged stance, abduction, and adduction were remained unchanged. In the simulation, the parameter of bone resorption and formation were represented with loading frequencies f_{ol}, f_{ab}, f_{ad}, and $f_{unloading}$ as Eqs. (13) ~ (15). In the cane-assisted walking, we referred to the study on relative changes in muscle activity and kinetics during cane-assisted walking (Neumann et al., 1998). The cane use reduced the demand on the hip abductors and decreased joint compression forces related to muscle contraction in the contralateral side. We calculated joint force and hip abductor force at various rates of leaning force when using a cane (Fig. 6). That is, in the infrequent walking, the number of loading cycles per day decreased from the daily-loading condition (Table 1), while the same loading forces were applied to the femur; in the cane-assisted walking, the numbers of loading cycles per day remained unchanged but the loading forces were altered from the daily-loading condition (Kwon et al., 2010b).

$$\Gamma_c = \frac{f_{ol}\Gamma_{c\_ol} + f_{ab}\Gamma_{c\_ab} + f_{ad}\Gamma_{c\_ad}}{f_{ol} + f_{ab} + f_{ad} + f_{unloading}} \tag{13}$$

$$AF_r = \frac{f_{ol}AF_{r\_ol} + f_{ab}AF_{r\_ab} + f_{ad}AF_{r\_ad}}{f_{ol} + f_{ab} + f_{ad} + f_{unloading}} \tag{14}$$

$$AF_f = \frac{f_{ol}AF_{f\_ol} + f_{ab}AF_{f\_ab} + f_{ad}AF_{f\_ad}}{f_{ol} + f_{ab} + f_{ad} + f_{unloading}} \tag{15}$$

The trabecular structure of the human proximal femur under the infrequent walking condition was shown for each rate of unloading interval and the initial, i.e., normal trabecular structure was also shown in Fig. 7. In the initial structure of Fig. 7(a), visible are all the normal groups of trabecular (Fig. 8), i.e. the compressive and tensile trabecular bones cross each other and the upper end of femur is completely occupied by cancellous tissue. Even Ward's triangle shows some thin trabecular bone (Singh et al., 1970).

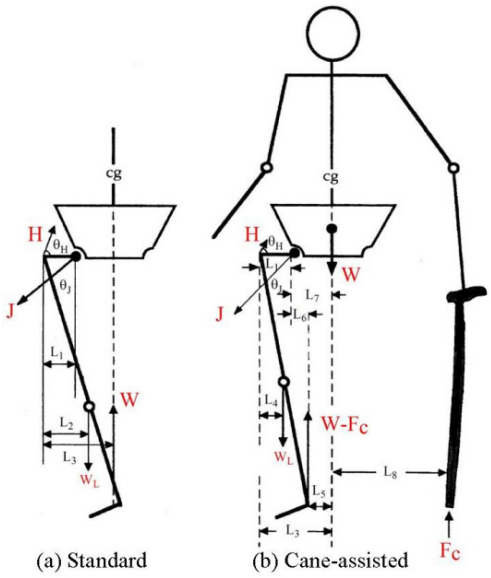

Figure 6. Diagram for boundary conditions of cane-assisted walk.

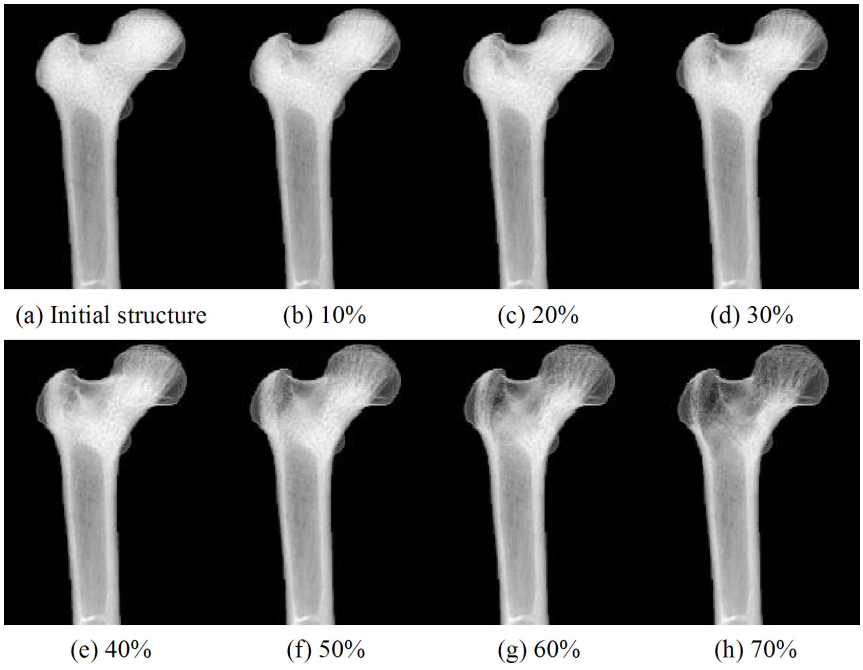

Figure 7. Simulated trabecular structure under infrequent walking.

Increasing the rate of unloading interval led to the increased bone loss, first in the femoral head and the greater trochanter. Ward's triangle was emptier in the case of higher rate of unloading frequency. Subsequently, the secondary compressive group disappeared and the principal tensile group became thinner with further increasing of the rate of unloading. When unloading level increased up to 70%, the principal compressive group little remained although the greater trochanter group was still observed clearly.

Figure 9 shows the trabecular structure changes under cane-assisted walking conditions. Using cane decreased joint compression forces related to muscle contraction in the contralateral side. Bone loss attracts attention on the greater trochanter group and Ward's triangle became clear when reducing hip abductor forces. Subsequent disappearing of the secondary compressive group and the thinning of the principal tensile group were observed with further increasing. This is similar to those observed for the infrequent walking. However, bone loss in the trabecular femoral head differed from that under the infrequent walking condition. The hip joint load will be involved in this difference.

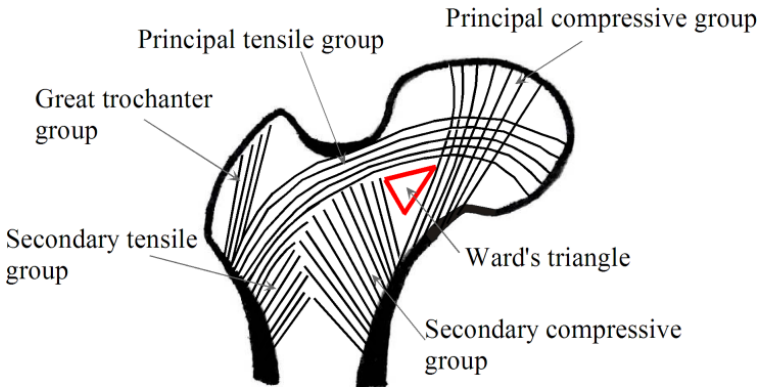

Figure 8. Trabecular structure pattern of human femur.

Clinically, the correlation of bed rest (reducing loading frequency) and muscle activity has been reported. The disuse due to bed rest with diseases accompanies with reduced muscle activity, and then leads to the cane use for walking. Thus, we simulated the trabecular remodeling by combining the two reduced weight-bearing conditions. Figure 10 shows that trabecular loss increased with increasing in the rate of unloading interval. Combination of reductions of loading frequency and loading forces relatively accentuated the structure of principal compressive and principal tensile groups and enhanced the thinning of the secondary compressive trabecular bone. Therefore, empty Ward's triangle is clearly observed. Further increase in the rate of unloading interval led to a marked reduction of tensile trabecular bone and discontinued the principal tensile group. Thus, the tensile trabecular bone is observed only in the upper part of the femoral head, where trabeculae are still comparable in density to the principal compressive trabeculae. Finally, even the principal compressive group became less obvious.

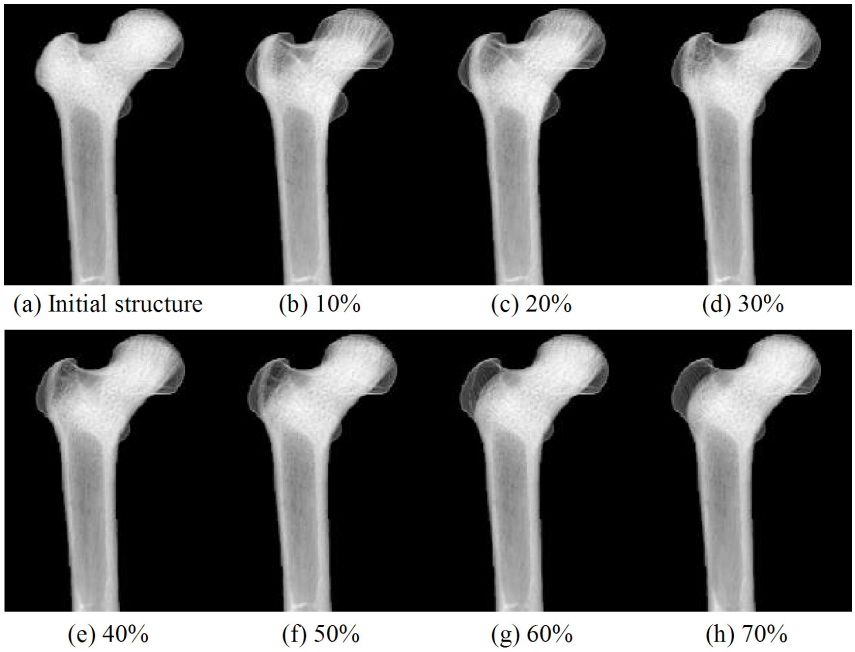

Figure 9. Simulated trabecular structures under cane-assisted walking

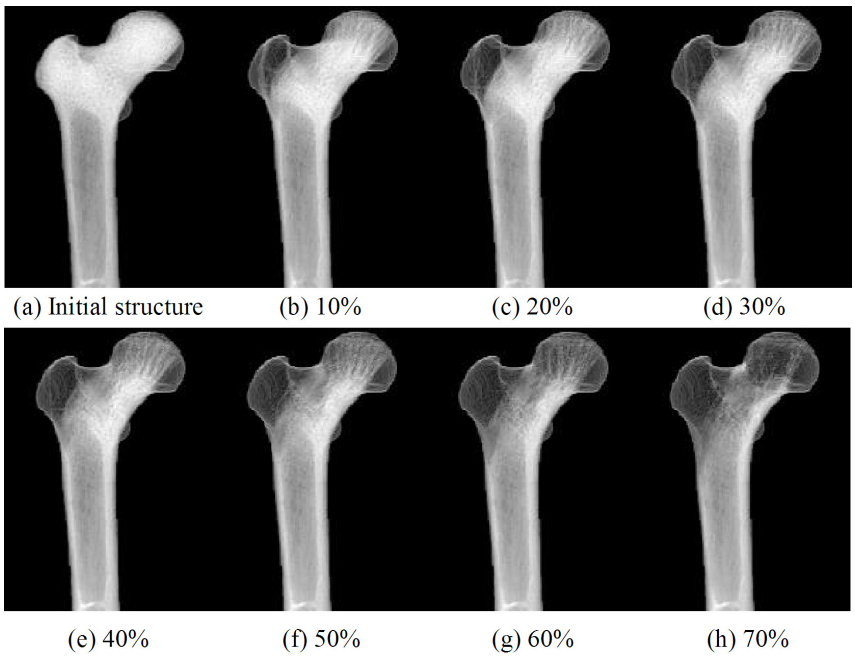

Figure 10. Simulated trabecular structures under infrequent cane-assisted walking.

Trabecular structure of the proximal femur is remodeled differently in response to various forms of mechanical stimulation (Wolff, 1986; Carter, 1987). In this study, we investigated that the structure changes of human trabecular bone under the reduced weight-bearing conditions by a surface remodeling model (Kwon et al., 2010a), in which osteocyte apoptosis plays a crucial role below a physiological strain range (Gu et al., 2005). The reduced weight-bearing conditions were imposed by assuming infrequent and/or cane-assisted walking. Depending on the reduced weight-bearing conditions, the trabecular structure reached different equilibrium structures even if the same initial structure and model parameters are used. In all cases, trabecular bone loss occurred in relation to the mechanical stimuli, although there was a regional difference in the pattern of bone loss between the two conditions. In the infrequent and cane-assisted walking conditions, significant bone loss occurred in the great trochanter and in the femoral head, respectively.

In the results of imposing the condition combining two reduced weight-bearing conditions, we found out the clinically observed trabecular structure in osteoporotic human proximal femur. The description for degree of osteoporotic trabecular structure (Singh Index) is shown in Table 2. The present stimulations showed that decreasing mechanical stimuli enhanced the degree of osteoporosis along with the grade defined by Singh et al. (1970). Figure 10 shows trabecular loss at various degrees of unloading. In the initial structure (Fig. 10 (a)), all groups of trabecular bones are visible, which corresponds to Grade 6 in Singh index. The compressive and tensile trabeculae intersect each other and the upper end of the femur is completely occupied by cancellous rich structure. Ward's triangle is not clearly delineated and there are some thin trabeculae in it. With increasing the proportion of unloading, there occurs an apparent accentuation of the structure of the principal compressive and principal tensile groups, while the secondary compressive trabeculae became thinner (Grade 5, Fig. 10 (b)~(c)). As a result, an empty region appears in Ward's triangle. Further increase in the proportion of unloading leads to the marked reduction in the tensile trabecular bones (Grade 4, Fig. 10 (d)~(e)); in due course, discontinuity occurs in the principal tensile group. At the stages of Fig. 10 (e) and (f), the tensile trabeculae are seen

Grade 6	All the normal trabecular groups are visible and the upper end of the femur seems to be completely occupied by trabecular bone.
Grade 5	The structure of principal tensile and principal compressive trabeculae is accentuated. Ward's triangle appears prominent.
Grade 4	Principal tensile trabeculae are markedly reduced in number but can still be observed in lateral cortex to the upper part of the femoral neck.
Grade 3	There is a break in the continuity of the principal tensile trabeculae opposite the greater trochanter. This grade indicates definite osteoporosis.
Grade 2	Only the principal compressive trabeculae stand out prominently; the others have been resorbed more or less completely.
Grade 1	Even the principal compressive trabeculae are markedly reduced in number and are no longer prominent.

Table 2. Singh Index

only in the upper part of the femoral head, where the trabeculae are still comparable in density to the principal compressive trabeculae (Grade 3). Finally, even the principal compressive group ceases to stand out (Grade 2, Fig. 10 (g)) and decreases markedly in number (Grade 1, Fig. 10 (h)). Therefore, the present remodeling model has the competence to study the trabecular bone loss in disuse-mediated osteoporosis, where bone resorption-dominant remodeling due to less mechanical stimuli should be characterized reasonably and sufficiently. That is introduced into the present model by considering the effect of osteocyte apoptosis under low strain stimuli, and it is essential in predicting the osteoporotic change of trabecular bone structure.

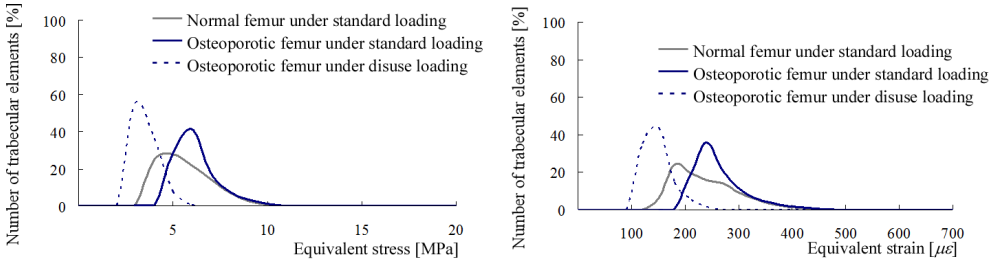

Figure 11. Equivalent stress and strain distributions in normal and osteoporotic femurs.

Finite element analyses were conducted for normal and osteoporotic human femurs obtained by remodeling simulation, and trabecular bone stress and strain were examined for a spherical volume of interest in the femoral head (Rietbergen et al., 2003). Figure 11 shows the distribution of voxel at different stress/strain for the normal femur of Fig. 10(a) and an osteoporotic femur of Fig. 10 (b) that is obtained under the disuse loading condition of reduced loading frequency and force. Solid and broken blue lines distinguish the stress/strain distribution for osteoporotic femur under standard and disuse loading conditions, respectively. Trabecular bone stress and strain in the osteoporotic femur were distributed more uniformly than those in the normal femur. In the osteoporotic femur, trabecular bones orthogonal to the alignment of the principal compressive group (non-principal trabeculae) are relatively-scarce because osteocytes in those trabeculae, especially in non-principal group originally exposed to relatively small loading, are susceptible to apoptosis when subjected to the disuse condition, resulting in scarcely distributed non-principal trabeculae. Consequently, trabeculae undergoing relatively-low stress/strain decrease and the peaks of stress and strain distributions increased in the osteoporotic femur. Trabeculae in principal compressive group are likely to preserve their role of relatively high load-bearing even under the disuse condition.

3.4. Importance of osteocyte apoptosis-induced bone resorption in remodeling simulation

To evaluate the advantage of including low and high strain ranges, we performed the simulation assuming the response model defined for physiological strain range to the entire strain range including low and high strain ranges, referred to physiological response-only

model hereafter. Results by physiological range-only model were compared with that obtained by the present integrated model considering individual response model for low and high strain ranges. This physiological response-only model determines the trabecular structure only by relative non-uniformity of strain distribution over all the strain range with no local acceleration of bone resorption and formation. Figure 12(a) shows the distribution of initial equivalent strain. Diaphyseal structure was formed with the loss of trabecular bone both integrated and physiological response-only models (Fig. 12(b)). However, bone resorption occurred to the higher degree in the integrated model, especially in low strain regions as clearly shown in dashed circles of Fig. 12(b). Figure 13 shows the simulation result for change of volume fraction in ward's triangle region at each model. The integrated model was reached to equilibrium state, faster than physiological response-only model. Ward's triangle region has a low strain range, as seen in Fig. 12(a). Figure 14 shows the histogram of number of trabecular bone elements against initial equivalent strain distribution for both simulation models. In the low strain range below $100\mu\varepsilon$, as much as 43, 37, and 46% of trabecular bone preserved in the physiological response-only model were resorbed by the integrated model in different subjects of #1, #2, and #3, respectively. In low strain regions at the initial, the integrated model could reproduce more suitable trabecular structure by taking the characteristic response in low strain range into account. Furthermore, the correlation between bone volume fraction simulated and bone mineral density by CT image was higher in the integrated model than that in the physiological response-only model (Fig. 15).

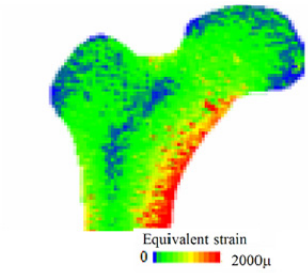

(a)Equivalent strain distribution of initial structure of Fig. 10(a)

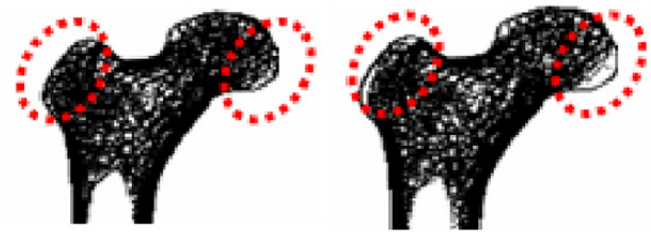

(b) Structure by physiological response-only model

(c) Structure by integrated model

Figure 12. Initial stress distribution and simulated trabecular structures.

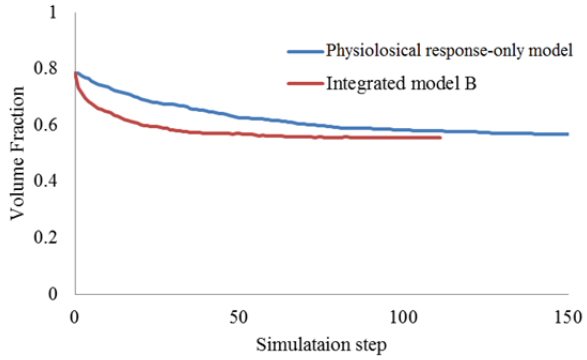

Figure 13. Volume fraction in Ward's triangle during remodeling simulation.

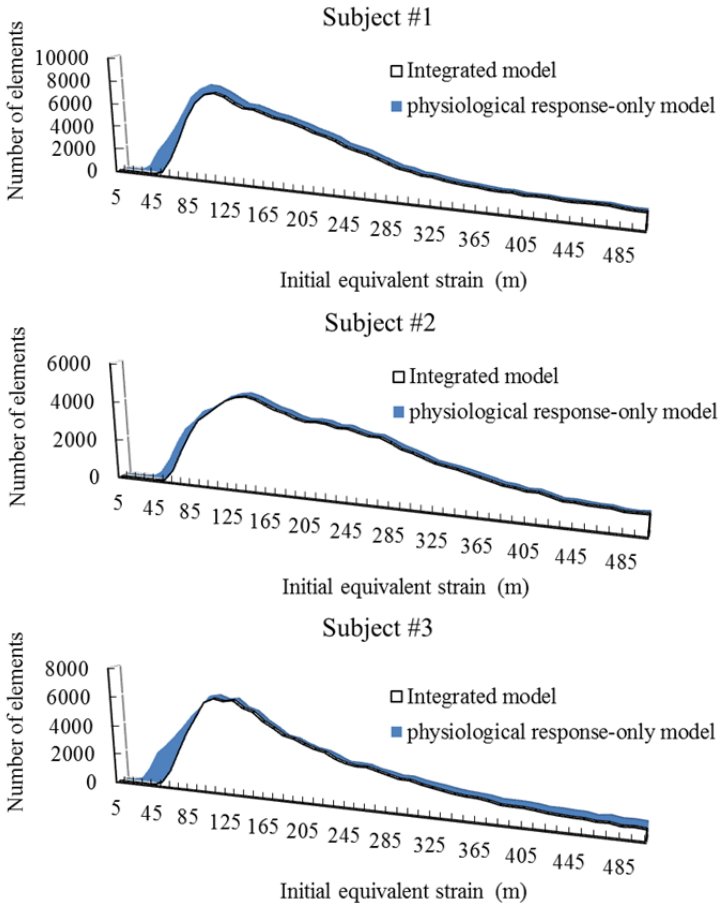

Figure 14. Number of trabecular bone elements in simulated proximal femur against initial equivalent strain levels before disuse-mediated remodeling.

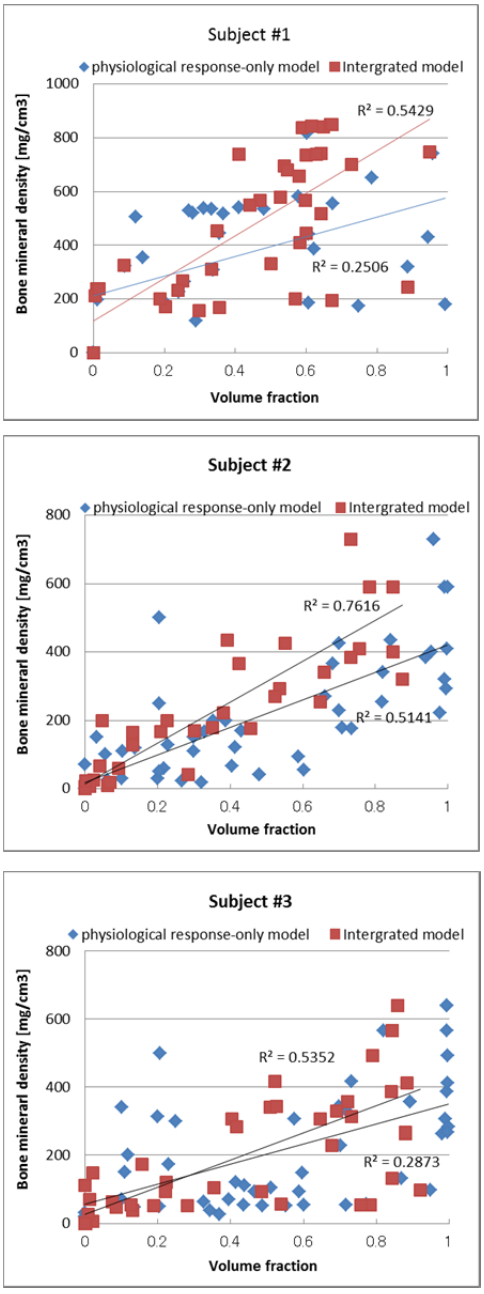

Figure 15. Bone mineral density at proximal femur by CT and simulated volume fraction by integrated and physiological response-only models.

4. Conclusions

In this chapter, described was the mathematical model of bone remodeling extending the established previously (Adachi et al., 1997) based on the mechanostat theory (Duncan & Turner, 1995; Frost, 2003; Hughes et al., 2010). Extension was the bone resorption-dominant response in low strain range by disuse and formation-dominant response in overuse windows. The osteocyte apoptosis in the low strain range due to weightlessness was a key aspect in the extended model, and the targeted remodeling was in the high strain range for bone formation. Trabecular structure in human proximal femur was simulated using the model extended and the reproduced trabecular structure exhibited good agreement with that in the actual femur more reasonably by taking the osteocyte apoptosis in low strain range and the targeted remodeling in high strain range. Especially, the consideration of osteocyte apoptosis was crucial in the mathematical model of bone remodeling model in reproducing the healthy normal bone structure and in simulation the disuse-mediated osteoporotic bone structure. The former was demonstrated by comparison of simulated volume fraction and the X-ray CT bone mineral density. For the latter, disuse-accelerated bone loss was examined for infrequent and cane-assisted walking conditions. The osteoporotic trabecular structure was examined in terms of Singh Index, a diagnostic criterion for the stage of progression of osteoporosis. This competence of the model was coming from the effect of osteoporosis due to less mechanical stimulus and its result of bone loss acceleration, and the present remodeling model is effective in bone remodeling simulation under reduced loading condition.

In conclusion, the effect of osteocyte apoptosis on bone resorption is inevitable aspect in the computer simulation of bone remodeling.

Author details

Ji Yean Kwon, Hisashi Naito, Takeshi Matsumoto and Masao Tanaka
Graduate School of Engineering Science, Osaka University, Japan

5. References

Adachi, T., Tomita, Y., Sakaue, H. & Tanaka, M., (1997), Simulation of trabecular surface remodeling based on local stress nonuniformity, *JSME International Journal*, *Series C*, Vol. 40, No. 4, pp. 782-792

Adachi, T., Tsubota, K., Tomita, Y. & Hollister, S.J., (2001), Trabecular surface remodeling simulation for cancellous bone using microstructural voxel finite element models, *Journal of Biomechanical Engineering*, Vol. 123, pp. 403-409

Baiotto, S., Labat B., Vico, L. & Zidi, M., (2009), Bone remodeling regulation under unloading condition: Numerical investigations, *Computer in Biology and Medicine*, Vol. 39, pp. 46-52

Barrera, G., Bunout, D., Gattás, V., Maza, M.P., Leiva, L. & Hirsch, S., (2004), A high body mass index protects against femoral neck osteoporosis in healthy elderly subjects, *Nutrition*, Vol. 20, No. 9, pp. 769-771

Beaupré, G.S., Orr, T.E. & Carter, D.R., (1990), An approach for time-dependent bone modeling-application: a preliminary remodeling simulation, *Journal of Orthopedic Research*, Vol. 8, pp. 662-670

Burr, D.B., (2002), Targeted and nontargeted remodeling, *Bone*, Vol. 30, No. 1, pp. 2-4

Caillot-Augusseau, A., Lafage-Proust. M.H., Soler, C., Pernod, J., Dubois, F. & Alexandre, C., (1998), Bone formation and resorption biological markers in cosmonauts during and after a 180-day space flight (Euromir 95), *Clinical Chemistry*, Vol. 44, pp.578–585

Carter, D.R., (1987), Mechanical loading history and skeletal biology, *Journal of Biomechanics*, Vol. 20, pp. 1095-1109

Cowin, S.C., (2001), *Bone mechanics handbook* (second edition), CRC press LLC, ISBN 0-8493-9117-2, USA

Da Costa Gómez, T.M., Barrett, J.G., Sample, S.J., Radtke, C.L., Kalscheur, V.L., Lu, Y., Markel, M.D., Santschi, E.M., Scollay, M.C. & Muir, P., (2005), Up-regulation of site-specific remodeling without accumulation of microcracking and loss of osteocytes, *Bone*, Vol. 37, No. 1, pp. 16-24

Delgado-Calle, J., Arozamena, J., García-Renedo, R., García-Ibarbia, C., Pascual-Carra, M.A., González-Macías, J. & Riancho, J.A., (2011), Osteocyte deficiency in hip fractures, *Calcified Tissue International*, Vol. 89, pp.327-334

Duncan, R.L. & Turner, C.H., (1995), Mechanotransduction and the functional response of bone to mechanical strain, *Calcified Tissue International*, Vol. 57, No.5, pp. 344-358

Frost, H.M., (2003), Bone's mechanostat: a 2003 update, *The Anatomical Record, Part A, Discoveries in molecular, cellular, and evolutionary biology*, Vol. 275, No. 2, pp. 1081-1101

Fuchs, R.K,, Bauer, J.J. & Snow, C.M.,(2001), Jumping improves hip and lumbar spine bone mass in prepubescent children: a randomized controlled trial, *Journal of Bone Mineral Research*, Vol. 16, No. 1, pp.148–156

Garber, M.A., McDowell, D.L. & Hutton, W.C., (2000), Bone loss during simulated weightlessness: a biomechanical and mineralization study in the rat model, *Aviation Space Environmental Medicine*, Vol. 71, pp. 586–592

Gu, G., Mulari, M., Peng, Z., Hentuen, T.A. & Väänänen, H.K., (2005), Death of osteocytes turns off the inhabitation of osteoclasts and triggers local bone resorption, *Biomechanical and Biophysical Research Communications*, Vol. 335, No. 4, pp. 1095-1101

Hughes,J.M. & Petit, M.A.,(2012), Biological underpinnings of Frost's mechanostat thresholds:The important role of osteocytes, *Journal of Musuloskelet Neuronal Interact*, Vol. 10, No. 2, pp. 128-135

Kaneps A.J., Stover S.M. & Lane N.E., (1997), Changes in canine cortical and cancellous bone mechanical properties following immobilization and remobilization with exercise, *Bone*, Vol. 21, pp. 419–423

Kennedy, O.D., Herman, B.C., Laudier, D.M., Majeska, R.J., Sun, H.B. & Schaffler, M.B., (2012), Activation of resorption in fatigue-loaded bone involves both apoptosis and active pro-osteoclastogenic signaling by distint osteocyte popuations, *Bone*, Vol. 50, pp. 1115-1122

Klein-Nulend, J., Bacabac, R.G. & Mullender M.G., (2005), Mechanobiology of bone tissue, *Pathologie Biologie*, Vol. 53, pp. 576-580

Kwon, J.Y., Naito, H., Matsumoto, T. & Tanaka, M., (2010a), Simulation model of trabecular bone remodeling considering effects of osteocytes apoptosis and targeted remodeling, *Journal of Biomechanical Science and Engineering*, Vol. 5, No. 5, pp. 539-551

Kwon, J.Y., Naito, H., Matsumoto, T. & Tanaka, M., (2010b), Computational study on trabecular bone remodeling in human femur under reduced weight-bearing conditions, *Journal of Biomechanical Science and Engineering*, Vol. 5, No. 5, pp. 552-564

Lang, T., LeBlanc, A., Evans, H., Lu Y., Genant, H. & Yu, A., (2004), Cortical and trabecular bone mineral loss from the spine and hip in long-duration spaceflight, *Journal of Bone Mineral Research*, Vol. 19, pp. 1006– 1012

LaMonte, J.M., Hamilton, N.H. & Zernicke, R.F., (2005), Strain rate influences periosteal adaptation in mature bone, *Medical Engineering & Physics*, Vol. 27, pp.277-284

LeBlanc, A.D., Schneider, V.S., Evans, H.J., Engelbretson, D.A. & Krebs, J.M., (1990), Bone mineral loss and recovery after 17 weeks of bed rest, *Journal of Bone and Mineral Research*, Vol. 5, pp. 843–850

Li, C.Y., Majeska, R.J., Laudier, D.M., Mann, R. & Schaffler, M.B., (2005), High-dose risedronate treatment partially preserves cancellous bone mass and microarchitecture during long-term disuse, *Bone*, Vol. 37, pp. 287–295

Luo, G., Cowin, S.C., Sadegh, A.M. & Arramon, Y.P., (1995), Implementation of strain rate
as a bone remodeling stimulus, *Journal of Biomechanical Engineering*, Vol. 117, pp. 329-338

McGee, M.E., Maki, A.J., Johnson, S.E., Nelson, O.L., Robbins, C.T. & Donahue, S.W., (2008), Decreased bone turnover with balanced resorption and formation prevent cortical bone loss during disuse(hibernation) in Grizzly bears(Ursus arctos horribilis), *Bone*, Vol. 42, pp. 396-404

McKay, H.A., Petit, M.A., Schutz, R.W., Prior, J.C., Barr, S.I. & Khan, K.M., (2000), Augmented trochanteric bone mineral density after modified physical education classes: a randomized school-based exercise intervention study in prepubescent and early pubescent children, *Journal of Pediatrics*, Vol. 136, No. 2, pp.156–162

Noble, B.S., Peet, N., Stevens, H.Y., Brabbs, A., Mosley, J.R., Reilly, G.C., Reeve, J., Skerry, T.M. & Lanyon, L.E., (2003), Mechanical loading: biphasic osteocyte survival and targeting of osteoclasts for bone destruction in rat cortical bone, *American Physiological Society*, Vol. 284, No. 4, pp. C934-C943

Neumann, D.A., (1998), Hip abductor muscle activity as subjects with hip prostheses walk with different methods of using a cane, *Physical Therapy*, Vol. 78, pp. 490-501

Parfitt, A.M., (1994), Osteonal and hemi-osteonal remodeling: the spatial and temporal framework for signal traffic in adult human bone. *Journal of Cellular Biochemistry*, Vol. 55, pp. 273–286

Rietbergen, B., Huiskes, R., Eckstein, F. & Rüegsegger, P., (2003), Trabecular bone tissue strains in the healthy and osteoporotic human femur, *Journal of Bone and Mineral Research*, Vol. 18, No. 10, pp. 1781-1788

Ruimerman, R., Huiskes, R., Van Lenthe, G.H. & Janssen, J.D., (2001), A computer simulation model relating bone-cell metabolism to mechanical adaptation of trabecular bone, *Computational Methods in Biomechanical and Biomedical Engineering*, Vol. 4, pp. 433-448

Shackelford, L.C., LeBlanc, A.D., Driscoll, T.B., Evans, H.J., Rianon, N.J., Smith, S.M., Spector, E., Feeback, D.L. & Lai, D., (2004), Resistance exercise as a countermeasure to disuse-induced bone loss, *Journal of Applied Physiology*, Vol. 97, pp. 119–129

Singh, M., Nagrath, A.R. & Maini, P.S., (1970), Changes in Trabecular Pattern of the Upper end of the Femur as an index of osteoporosis, *The Journal of Bone and Joint Surgery*, Vol. 52, pp. 457-467

Sordia, L.H., Vazquez, J., Iglesias, J.L., Piñeyro, M.O., Vidal, O., Saldivar, D., Morales A., Merino, M. Pons, G. & Rosales, E., (2004), Low height and low weight correlates better with osteoporosis than low body mass index in postmenopausal woman, *International Congress Series*, Vol. 1271, pp. 407-410

Takata, S. & Yasui, N., (2001), Disuse osteoporosis, *The Journal of Medical Investigation*, Vol. 48, pp. 147–156

Tsubota, K., Adachi, T. & Tomita, Y., (2002), Functional adaptation of cancellous bone in human proximal femur predicted by trabecular surface remodeling simulation toward uniform stress state, *Journal of Biomechanics*, Vol. 35, pp. 1541-1551

Tsubota, K. & Adachi, T., (2006), Simulation study on local and integral mechanical quantities at single trabecular level as candidate of remodeling stimuli, *Journal of Biomechanical Science and Engineering*, Vol. 1, pp. 124-135

Tsubota, K., Suzuki, Y., Yamada, T., Hojo, M., Makinouchi, M. & Adachi, T., (2009), Computer simulation of trabecular remodeling in human proximal femur using large-scale voxel FE models: Approach to understanding Wolff's law, *Journal of Biomechanics*, Vol. 42, pp. 1088-1094

Vailas, A.C., Zernicke, R.F., Grindeland, R.E., Kaplansky, A., Durnova, G.N., Li, K.C. & Martinez, D.A., (1990), Effects of spaceflight on rat humerus geometry, biomechanics, and biochemistry. *The FASEB Journal*, Vol. 4, pp. 47–54

Vico, L., Collet, A., Guignandon, P., Lafage-Proust, M.H., Thomas T., Rehailia M. & Alexandre C., (2000), Effects of long term microgravity exposure on cancellous and cortical weight-bearing bones of cosmonauts, *The Lancet*, Vol. 355, pp. 1607-1611

Weinreb, M., Rodan, G.A. & Thompson, D.D.,(1989), Osteopenia in the immobilized rat hind limb is associated with increased bone resorption and decreased bone formation, *Bone*, Vol. 10, pp.187–194

Wolff, J., (1986), The Law of Bone Remodeling, *Springer (Trans. Maquet, P., Furlong, R.)*